# Numerical modeling of the deposition of combustion-generated soot particles on cold wall surfaces

**By Arnaud Trouvé†, Bénédicte Cuenot‡, Eleonore Riber‡**

The build-up of soot deposits on cold wall surfaces is a problem of unknown significance for combustion applications. Soot deposits are due to thermophoretic transport and are generally ignored in theoretical and numerical analysis. We examine here the relationship between the rate of soot deposition and the wall convective heat flux, using both direct numerical simulation (DNS) and large eddy simulation (LES), and a semi-empirical soot model. The soot model adopts an Eulerian approach in which the material properties for thermophoretic transport are independent of particle size. Numerical simulations are performed using two advanced research codes, les3d-mp and AVBP; The DNS of a laminar wall diffusion flame provides insights into the dynamics of soot deposits and leads to the development of a simple soot deposition model for wall-modeled LES. The performance of the subgrid-scale soot deposition model is then evaluated in LES of a soot-laden turbulent channel flow by comparing results from wall-resolved LES and wall-modeled LES. Initial results are encouraging and work is in progress to extend the present study to the case of turbulent non-premixed wall flames.

## 1. Introduction

In many combustion systems, the chemical pathways responsible for fuel oxidation and heat release are accompanied by the formation of undesirable by-products, for instance soot particles. In engine applications, soot is normally present in small quantities and while being a concern because of its negative effects on human health and the environment, soot has a limited impact on combustion dynamics. In contrast, in fire applications, soot is often present in large quantities (in large-scale pool fires, the soot yield may reach values of 15% or higher) and because it tends to dominate the radiant power of the flame, soot has a significant (and possibly dominant) impact on the combustion dynamics.

Remarkable progress has been made during the past two decades in our understanding of fundamental soot processes, including gas-phase soot precursors chemistry (*e.g.*, polycyclic aromatic hydrocarbons chemistry), particle nucleation (a gas-to-solid phase change occurring at the nanometer scale), particle mass growth and oxidation via gas-solid heterogeneous chemistry and aerosol dynamics (featuring particle coagulation and cluster formation that occur between the nanometer and micrometer scales). This progress has significantly improved our ability to mathematically model and numerically simulate soot processes in combustion systems.

One area, however, that has received relatively little attention is the problem of soot deposition on solid wall surfaces. Soot deposits are explained by thermophoretic transport effects, *i.e.* by the thermally-driven, diffusion-like transport of aerosol particles from

† Department of Fire Protection Engineering, University of Maryland, MD 20742,USA
‡ CERFACS, Toulouse, France

hot to cold regions. In engine applications, deposition of soot on the combustion chamber walls is usually considered as a minor problem: soot deposits on walls is a potential (minor) contributor to exhaust particulate emissions; in addition, soot deposits will change the wall emissivity and will result in increased rates of radiative heat transfer (soot deposits may also generate hot spots and result in increased thermal stresses). In contrast, in compartment fire applications, deposition of soot on walls is a problem of unknown significance: because the surface of contact between soot-laden combustion gases and compartment walls is often quite large (up to several 10s of square meters), deposition of soot particles may correspond to a significant mass sink term. The presence of soot deposits on walls is currently neglected in Computational-Fluid-Dynamics-based fire models.

Previous studies of soot deposition on solid wall surfaces include studies of laminar or turbulent, chemically-inert, particle-laden flows (Batchelor & Shen (1985); Makel & Kennedy (1990); Tsai & Lu (1955); He & Ahmadi (1998); Thakurta *et al.* (1998); Messerer *et al.* (2003); Nagendra *et al.* (2011)) and studies of laminar wall flames (Choi *et al.* (2006, 2008)). The objective of the present study is two-fold: to revisit some of these past studies and examine the relationship between the rate of soot deposition and the wall convective heat flux; and to extend the scope of previous studies to the case of turbulent non-premixed wall flames.

The present project uses both Direct Numerical Simulation (DNS) and Large Eddy Simulation (LES) combined with an Eulerian semi-empirical soot model. DNS results corresponding to a chemically-inert particle-laden laminar channel flow and a laminar wall flame are presented in Section 2; these results are obtained using a low Mach number solver called les3d-mp. LES results corresponding to a chemically-inert particle-laden turbulent channel flow are presented in Section 3; these results are obtained using a compressible flow solver called AVBP.

## 2. Direct Numerical Simulation

DNS simulations were performed using an in-house research code developed at the University of Maryland and called les3d-mp. les3d-mp was originally developed as a DNS/LES solver for turbulent boundary layer/channel flows by Keating *et al.* (2004) and was recently enhanced to treat variable mass density and combustion (Bravo (2012)) using a formulation proposed by Pierce (2001). les3d-mp is an incompressible Navier-Stokes solver based on a classical projection method and an implicit second-order time integration technique featuring an implicit iterative scheme to treat wall-normal diffusion and an explicit iterative scheme to treat convection and in-plane diffusion. Additional features include a second-order finite difference scheme for spatial discretization on a staggered computational grid, a direct matrix inversion solver for the pressure Poisson equation, and a parallel computing implementation based on Message Passing Interface (MPI) protocols. The combustion model is an equilibrium (*i.e.* infinitely fast-chemistry) model which uses a single-step global combustion equation and adopts mixture fraction and total enthalpy as principal variables; thermodynamic properties are taken from CHEMKIN databases.

### 2.1. *Soot model*

The soot model adopted in the present study corresponds to a full Eulerian approach (alternative Lagrangian particle approaches may be found in (He & Ahmadi (1998);

Thakurta *et al.* (1998); Nagendra *et al.* (2011)). The model adopts a simplified, phenomenological modeling strategy in which soot formation is described using two transport equations for soot mass fraction $Y_s$ and soot number density $n$ (Moss *et al.* (1995)):

$$\frac{\partial \rho Y_s}{\partial t} + \frac{\partial \rho Y_s u_i}{\partial x_i} = -\frac{\partial}{\partial u_i}\left(\rho Y_s V_{t,i}\right) + \dot{\omega}_s \ , \tag{2.1}$$

$$\frac{\partial}{\partial t}\left(\frac{n}{N_0}\right) + \frac{\partial}{\partial x_i}\left(\frac{n}{N_0}u_i\right) = -\frac{\partial}{\partial u_i}\left(\frac{n}{N_0}V_{t,i}\right) + \dot{\omega}_n \ , \tag{2.2}$$

where $\rho$ is the mixture mass density, $u_i$ ($V_{t,i}$) is the $x_i$-component of the flow (thermophoretic) velocity vector, $N_0$ is the Avogadro number, $\dot{\omega}_s$ is the net reaction rate for soot mass and $\dot{\omega}_n$ the net production rate for soot number density. The models for $\dot{\omega}_s$ and $\dot{\omega}_n$ incorporate semi-empirical descriptions of important physical and chemical soot processes, *e.g.* particle inception, surface growth, oxidation, and coagulation. Model coefficients are taken from Moss *et al.* (1995). These expressions are also based on a number of simplifying assumptions, for instance the model ignores the role of soot precursors and assumes a mono-dispersed soot particle size distribution.

Thermophoretic transport is included in Eqs. 2.1 and 2.2 via the velocity $V_{t,i}$. Thermophoresis corresponds to the thermally-driven transport of aerosol particles from hot to cold regions. A classical expression for the thermophoretic velocity is:

$$V_{t,i} = -0.54\frac{\mu}{\rho}\frac{\partial}{\partial x_i}\left(ln(T)\right) \ , \tag{2.3}$$

where $T$ is the temperature and $\mu$ is the dynamic viscosity. Equation 2.3 is derived from the kinetic theory of gases and is valid in the limit of small particles (*i.e.* in the free-molecular regime or roughly, for particle diameters much smaller than 70 nm). Fortunately, several studies suggest that Eq. 2.3 is also valid for large particles, including spherical particles with diameters up to at least 500 nm and particles with a complex cluster morphology (Tsai & Lu (1955); Messerer *et al.* (2003); Gomez & Rosner (1993)). Thus, Eq. 2.3 is believed to be adequate for a large fraction of the soot particles population. The corresponding expression for the mass flux in the $x_i$-direction is then:

$$\dot{m}_{s,i} = \rho Y_s V_{t,i} = -0.54\mu Y_s \frac{\partial}{\partial x_i}\left(ln(T)\right) \ . \tag{2.4}$$

When considered at a solid wall surface, Eq. 2.4 provides an expression for the rate of soot deposition (ROSD), noted $\dot{m}_{s,w}$. It also shows that ROSD is related to the wall convective heat flux (CHF), noted $\dot{q}_{w,c}$, as follows:

$$\dot{m}_{s,w} = 0.54\frac{\mu_w}{k_w}\frac{Y_{s,w}}{T_w}\dot{q}_{w,c} \ , \tag{2.5}$$

where $k$ is the thermal conductivity and the $w$ subscript designates wall conditions. This expression forms the basis of a model in which ROSD is correlated to CHF. As pointed out by Batchelor & Shen (1985), there are a few academic configurations that feature an analogy between transport of particles and transport of heat and in which $\dot{m}_{s,w}$ and $\dot{q}_{w,c}$ are linearly related. The relationship between ROSD and CHF in flame configurations is unknown.

### 2.2. *Numerical simulation of a particle-laden, laminar channel flow*

The implementation of the soot deposition boundary condition was verified by performing a test simulation corresponding to the thermophoretic precipitator configuration studied

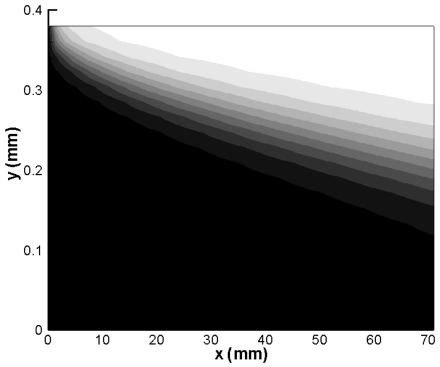


FIGURE 1. Soot mass fraction distribution inside the thermophoretic precipitator studied in Ref. [3] (les3d-mp simulation). The flow is steady and laminar, and is directed from left to right; $Y_s$ is normalized by its value at the inlet of the tube. Note that the picture does not respect the aspect ratio of the tube (the tube is long and narrow). Minimum value : white - $Y_s = 0$ ; maximum value : black - $Y_s = 1$.

experimentally by Tsai & Lu (1955). The configuration features a particle-laden air flow across a rectangular-shaped tube characterized by a constant and uniform temperature gradient in the cross-steam direction. The flow is a classical laminar Poiseuille flow (the volume flow rate is 0.4 l/min; the flow velocity is 0.585 m/s). The tube is long and narrow (and is 71 mm long, 0.38 mm high and 30 mm wide); the width of the tube is large and the flow and soot variations inside the tube are essentially two-dimensional. The walls of the tube are isothermal: the difference in temperature between the bottom (cold) and top (warm) walls is 19.1 K (the temperature gradient is 502.63 K/cm); this difference in temperature is small and buoyancy effects are neglected.

The experiment was performed using monodisperse solid sodium chloride particles; the experiment was repeated several times for particle sizes ranging from 40 to 500 nm. In contrast, the les3d-mp simulation treats soot particles with size-independent properties (see Eq. 2.3). The cross-stream temperature variation drives the thermophoretic migration of the solid particles from the top wall to the bottom wall. Figure 1 illustrates this effect and shows that the region near the top wall becomes progressively soot-free while the soot particles are absorbed on the bottom wall surface. The overall performance of the thermophoretic precipitator may be characterized by a particle collection efficiency $\eta$ defined as the ratio of the rate of particle deposition on the bottom wall divided by the rate of particle inflow at the inlet of the tube; the les3d-mp simulation gives a particle collection efficiency $\eta = 44\%$; this value is in good agreement with the experimental results of Tsai & Lu (1955) that range from 39.7% to 49.4%, with a slight decrease of $\eta$ with particle size.

### 2.3. *Numerical simulation of a laminar wall flame*

We now consider a representative laminar wall flame configuration. The configuration is similar (albeit not identical) to that considered in the experimental study presented by Choi *et al.* (2006, 2008). The configuration is two-dimensional and corresponds to a small diffusion flame fueled by a slow stream of ethylene injected into a flat plate boundary layer (see Fig. 2). The flat plate is located at $y = 0$. An air cross stream at ambient temperature flows parallel to the plate at a velocity $u_\infty$=0.6 m/s. Ethylene fuel is injected across a slot in the plate located 1 cm downstream of the leading edge, the width of the slot is 0.5 cm. The fuel mass flow rate is $\dot{m}_{f,w}$=18 g/s/m$^2$ (the fuel velocity is 1.55 cm/s; note that the

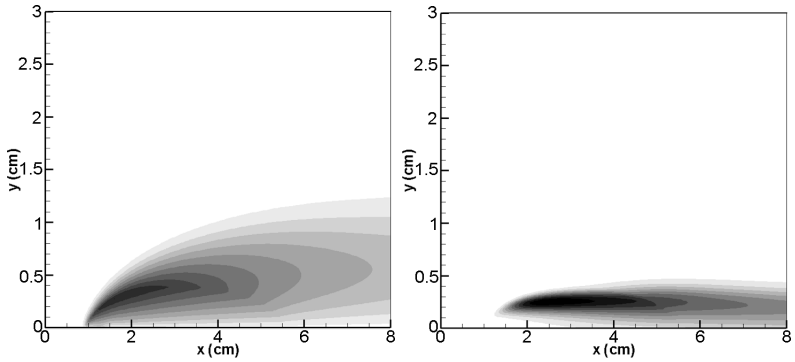


FIGURE 2. Spatial variations of temperature (left - maximum value : black, $T = 2400\,K$ - minimum value : white, $T = 400\,K$) and soot mass fraction (right - maximum value : black, $Y_s = 0.004$ - minimum value : white, $Y_s = 0$) in a boundary layer flame configuration (les3d-mp simulation). The air flow is directed from left to right; the solid plate is located at $y = 0$; ethylene fuel is injected at $y = 0$, for $1 \leq x \leq 1.5$ cm.

fuel-to-air momentum ratio is quite low, $\dot{m}_{f,w}/(\rho_\infty u_\infty)$=0.025); the plate temperature is $T_w$ = 300K and the injection slot is treated as adiabatic. The experimental study reported by Choi *et al.* (2006, 2008) was performed under micro-gravity conditions and accordingly, the les3d-mp simulation is performed without gravity.

Figure 2 shows that the flame is strongly affected by the momentum of the cross flow and is developing parallel to the solid plate. The flame (defined as the stoichiometric iso-contour) is approximately 5 cm long. The proximity of the flame to the wall creates large temperature gradients at the wall surface that in turn are responsible for strong thermophoretic velocities and high levels of soot deposition. In the simulation, 39% of the soot particles produced by the flame are absorbed on the wall (note that the computational domain does not contain the entire soot deposition region and soot deposition continues beyond the outflow boundary located at $x = 8\,cm$).

Figure 3 adopts a different perspective and examines the relationship between ROSD ($\dot{m}_{s,w}$) and CHF ($\dot{q}_{w,c}$). Figure 3 presents scatter plots of the wall thermophoretic velocity $V_{t,w}$ and ROSD as a function of CHF, for data taken downstream of the fuel slot, for $2 \leq x \leq$8 cm. Figure 3 shows that $\dot{q}_{w,c}$ takes values between 10 and 55 kW/m$^2$, $V_{t,w}$ takes values between 1 and 5.5 cm/s, and $\dot{m}_{s,w}$ takes values between 0.001 and 0.014 g/s/m$^2$. While Figure 3 shows the expected linear relationship between $V_{t,w}$ and $\dot{q}_{w,c}$ (this relationship is trivial in the case of an isothermal wall, see Section 2.1), it fails to reveal any correlation between $\dot{m}_{s,w}$ and $\dot{q}_{w,c}$. The variations of $\dot{m}_{s,w}$ are found to be complex and non-monotonic, and result from competing influences of $V_{t,w}$ and $Y_{s,w}$ ($V_{t,w}$ decreases with $x$ whereas $Y_{s,w}$ increases with $x$). This result suggests that a model that relates ROSD to CHF should use $V_{t,w}$ as the basis for the correlation and provide a separate estimate for $Y_{s,w}$. This idea will be used in the next section in the context of wall-modeled LES simulations.

## 3. Large Eddy Simulation of particle-laden turbulent channel flow

Most soot-laden flows of interest occur in turbulent environments. Due to combustion, temperature gradients are present in the entire volume of the burner but they are of particular importance in the boundary layer. Once soot particles are produced, their distribution is controlled by turbulent diffusion in the combustion chamber volume, and by

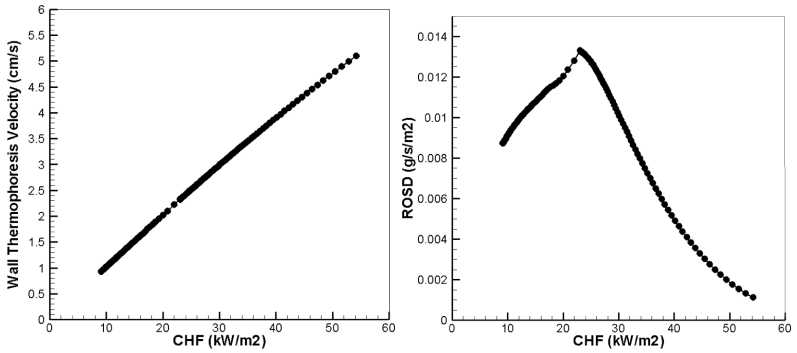


FIGURE 3. Scatter plot of the wall thermophoresis velocity (left) and the rate of soot deposition ROSD (right) versus the wall convective heat flux CHF (les3d-mp simulation).

thermophoresis in the turbulent boundary layers near the chamber walls. Both mechanisms interact in a combined process where turbulent diffusion feeds the boundary layer with soot coming from the bulk flow, which then deposits on walls by thermophoresis. To study this mechanism, Wall-Resolved Large Eddy Simulation (WRLES) of thermophoresis in a periodic turbulent channel was performed. The same configuration was then computed with a Wall-Modeled Large Eddy Simulation (WMLES) approach to propose a modelling strategy suitable for practical combustion systems. Walls are isothermal, either treated with a no-slip boundary condition in the WRLES case, or a classical law of the wall in the WMLES case.

The configuration studied in this section is a channel of square section $30\,mm$ x $30\,mm$ and length $60\,mm$. It is filled with air at a mean temperature of 350K, while the channel walls are at 320K, leading to a significant temperature gradient in the turbulent thermal boundary layer. The channel is periodic in the axial and transverse $x$ and $z$-directions, and a pressure gradient is imposed to maintain a bulk flow at a mean velocity of $70\,m/s$, corresponding to a Reynolds number $Re$ of the order of 200,000. Similarly, the temperature field is maintained in the channel thanks to an energy source term added to the energy conservation equation.

The two hexahedral meshes used for WRLES and WMLES have similar cell sizes in the interior of the domain, but the WRLES mesh is refined near the walls to reach the condition $y^+ = 1$ at the wall, while $y^+$ is between 20 and 70 in the WMLES uniform mesh. Therefore the core turbulent flow and mixing will be the same in both cases and differences will only appear in the turbulent boundary layer where thermophoresis occurs. The meshes count 97 x 131 x 97 nodes in the WRLES case and 97 x 97 x 97 nodes in the WMLES case, leading to a typical cell size of 300 $\mu$m in both cases but a much smaller minimum cell size of 5 $\mu$m at the wall in the WRLES case.

Simulations were performed with the AVBP code, jointly developed by CERFACS and IFPEN (Institut Français du Pétrole Energies Nouvelles) to simulate turbulent reacting flows in complex industrial geometries (Selle *et al.* 2004; Boileau *et al.* 2008; Wolf *et al.* 2012). AVBP solves the fully compressible Navier-Stokes equations together with chemical species conservation equations. It includes realistic thermochemistry and two-phase flow solvers (Eulerian and Lagrangian). The set of equations is solved with a third-order finite volume approach on unstructured grids (Colin & Rudgyard 2000). The code uses domain decomposition to run in parallel and has demonstrated excellent scalability on a large number of processors. The Smagorinsky model and the Wall Adaptive Local Eddy-

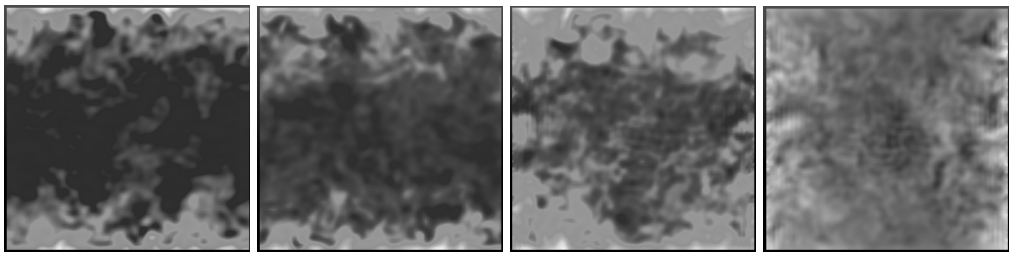

FIGURE 4. Instantaneous cuts of the soot mass fraction from WMLES field at $t = 0.71\,s$; $1.92\,s$; $5.93\,s$; $7.43\,s$ (from left to right, AVBP simulation).

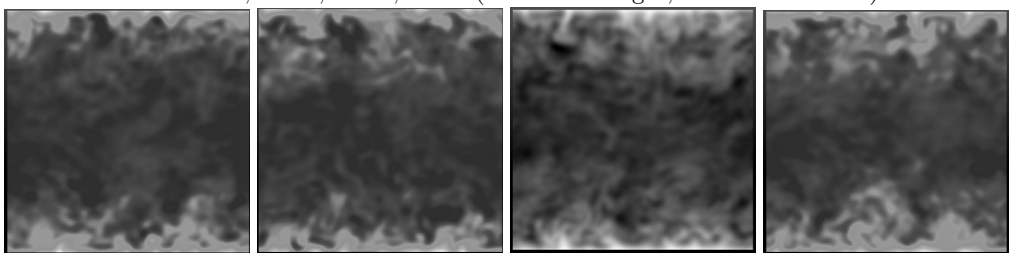

FIGURE 5. Instantaneous cuts of the temperature field from WMLES at $t = 0.71\,s$; $1.92\,s$; $5.93\,s$; $7.43\,s$ (from left to right, AVBP simulation).

Viscosity (Nicoud & Ducros 1999) are used for the sub-grid turbulent viscosity in the WMLES and the WRLES respectively.

The simulations are initialized with a well established anisothermal periodic flow, seeded with soot particles initially distributed through uniform soot mass fraction and number density fields. The soot model described by Eqs. 2.1 and 2.2 is used, where thermophoretic velocity is calculated from the heat flux vector as in Eq. 2.5. We now turn to the modeling of soot deposition in WMLES. As seen in Eq. 2.5, a wall model for ROSD requires model expressions for both CHF and $Y_{s,w}$. In WMLES, the wall heat flux CHF is taken from the law of the wall; we choose also to simply estimate $Y_{s,w}$ by the value taken by the soot mass fraction in the first off-wall grid cell (this choice implicitly assumes small variations of $Y_s$ in the near-wall region; this choice will be re-visited in future work).

Figure 4 shows cuts of instantaneous fields of soot obtained at different times in the WMLES case. With thermophoresis, the soot conservation equation is similar to the temperature equation with isothermal boundary condition, and indeed both fields look very similar at the beginning, as may be seen from Fig. 5. However there is no compensating source term in the soot equation as in the energy equation and after some time, both fields start to differ, as soot gradually deposits at the wall.

The accuracy of the wall-modeled simulation is evaluated in Fig. 6(left) which shows a comparison of the time evolution of the mean soot mass fraction in WMLES and WRLES. The mean soot mass fraction is directly proportional to the thermophoresis wall flux, modeled in the WMLES with the law-of-the-wall heat flux. Results are very similar, and only a slight difference appears in the slope of the soot mass fraction decrease. The discrepancy comes from the difference in the wall soot mass fraction, smaller in the DNS case because of the smaller cell size at the wall (see Fig. 6(right)): when the simulation starts, the gradient of the thermophoretic velocity at the wall is much higher in the WRLES, resulting in a higher sink term for soot, therefore a faster decrease of soot mass

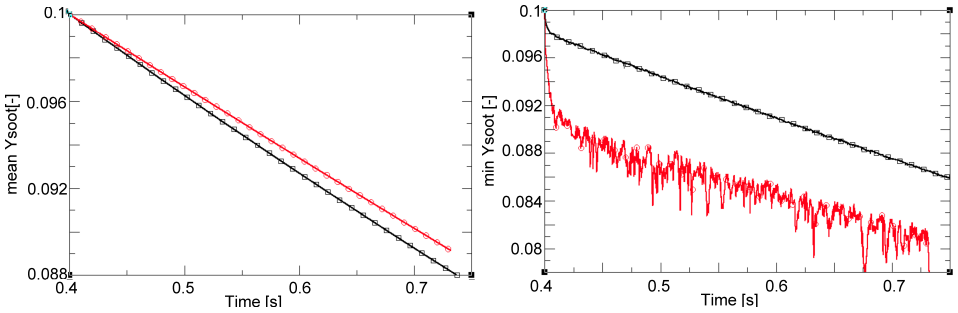


FIGURE 6. Left: Time evolution of the mean soot mass fraction from WRLES (squared red) and WMLES (circled black). Right: Time evolution of the minimum soot mass fraction from WRLES (squared red) and WMLES (circled black) (AVBP simulation).

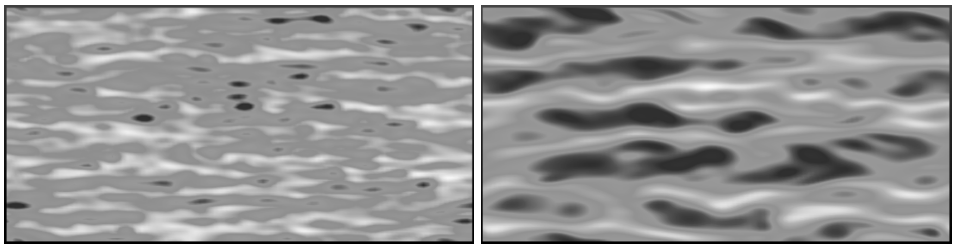

FIGURE 7. Instantaneous wall thermophoretic velocity from WRLES (left, maximum value: dark, 0.01 m/s) and WMLES (right, maximum value: dark, 0.009 m/s) (AVBP simulation).

fraction at the walls. This increased soot mass fraction gradient at walls in the WRLES then tends to compensate the higher thermophoretic velocity gradient, and after a short time the wall soot mass fraction decreases with the same slope in both WRLES and WMLES, maintaining the difference established at the beginning. The comparison of the wall thermophoretic velocity of Fig. 7 confirms that the law-of-the-wall gives a correct estimation of the wall heat flux and can be used for the thermophoretic velocity.

Because of the high CPU cost of the WRLES, only the WMLES case has been continued until all soot has deposited on walls and disappeared from the simulation domain. In Fig. 8(left), the time evolution of the mean soot mass fraction in a log-linear plot shows two phases: in a first phase, until approximately 6 $s$, soot decreases exponentially at a constant rate controlled by the wall thermophoretic velocity; in a second phase, the decrease strongly accelerates and the mean soot mass fraction goes rapidly to zero. To understand this behavior, spatially averaged (in the homogeneous directions $x$ and $z$) profiles of the soot mass fraction are plotted at different times in Fig. 8(right). In the first phase, and as already mentioned, the profiles of soot are similar to those of mean temperature, *i.e.* exhibit a maximum plateau at the center and a significant decrease near walls. This decrease is the result of the increasing thermophoretic flux, which keeps a positive slope when approaching the walls thanks to the sharp increase of the thermophoretic velocity. At the same time, turbulent diffusion transports soot from the center of the channel towards the walls. As later times, the profiles become flatter, under the combined effect of a smaller thermophoretic flux, which decreases with time as $Y_{s,w}$, and turbulent diffusion. After approximately 6 $s$, the mean soot mass fraction profiles are quasi-uniform. The competition between turbulent diffusion and thermophoresis becomes then strongly unbalanced, resulting in an acceleration of the decrease of the mean

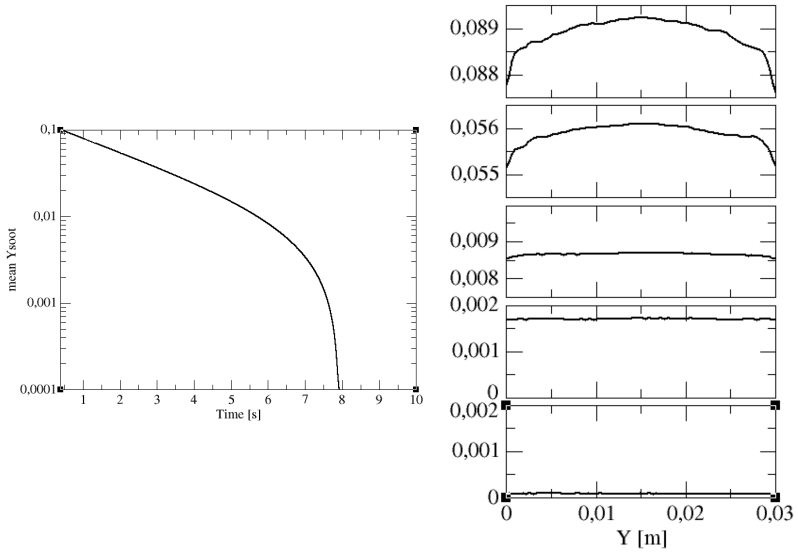


FIGURE 8. Left: Time evolution of mean soot mass fraction from the WMLES computation (AVBP simulation); Right: Spatially averaged profiles of soot mass fraction from the WMLES computation. From top to bottom, $t = 0.71\,s$; $1.92\,s$; $5.93\,s$; $7.43\,s$; $8.03\,s$ (AVBP simulation).

soot mass fraction, until complete disappearance. This acceleration starts when there is no sufficient soot remaining in the channel to compensate for thermophoretic deposition on walls.

## 4. Conclusions

The problem of soot deposition on cold wall surfaces is examined in the present study by performing DNS of laminar wall flames and LES of particle-laden turbulent channel flows. The results suggest that soot deposits are a major feature of elevated temperature sooty flows in contact with cold wall surfaces; for instance, the laminar wall flame simulation suggests that most of the soot particles produced by combustion are transported to, and absorbed on the wall surface. Both DNS and LES simulations feature thermophoretic velocities on the order of 1 cm/s; large values of $V_{t,w}$ result from large values of the wall temperature gradients. In the case of laminar wall flames, these large values are achieved because of large variations in temperature, whereas in the case of turbulent channel flows, large values are achieved because of small turbulent length scales. Furthermore, a simple soot deposition model is proposed for wall-modeled LES simulations. This model is based on a simple relationship between thermophoretic velocity and conduction heat flux, a classical turbulent model for the wall convective heat flux, and a model for the wall soot mass fraction. Preliminary results are encouraging and work is currently in progress to further evaluate the proposed model. Future work also includes the simulations of turbulent wall flames.

## REFERENCES

BATCHELOR, G. & SHEN, C. 1985 Thermophoretic deposition of particles in gas flowing over cold surfaces. *J. Colloid and Interface Science* **107**, 21–37.

Boileau, M., Pascaud, S., Riber, E., Cuenot, B., Gicquel, L., Poinsot, T. & Cazalens, M. 2008 Investigation of two-fluid methods for large eddy simulation of spray combustion in gas turbines. *Flow, Turbulence and Combustion* **80**, 291–321.

Bravo, L. 2012 Large eddy simulation of boundary layer combustion. PhD thesis, University of Maryland, College Park, USA.

Choi, J.-H., Fujita, O., Tsuiki, T., Kim, J. & Chung, S. 2006 In-situ observation of the soot deposition process on a solid wall with a diffusion flame along the wall. *JSME Intl. J., Series B-Fluids and Thermal Engineering* **49**, 167–175.

Choi, J.-H., Fujita, O., Tsuiki, T., Kim, J. & Chung, S. 2008 Experimental study in thermophoretic deposition of soot particles in laminar diffusion flames along a solid wall in microgravity. *Experimental Thermal and Fluid Science* **32**, 1484–1491.

Colin, O. & Rudgyard, M. 2000 Development of High-Order Taylor–Galerkin Schemes for LES. *Journal of Computational Physics* **162** (2), 338–371.

Gomez, A. & Rosner, D. 1993 Thermophoretic effects on particles in counterflow laminar diffusion flames. *Combust. Sci. Technol.* **89**, 355–362.

He, C. & Ahmadi, G. 1998 Particle deposition with thermophoresis in laminar and turbulent duct flows. *Aerosol Sci. Technol.* **29**, 525–546.

Keating, A., Piomelli, U., Bremhorst, K. & Nesic, S. 2004 Large-eddy simulation of heat transfer in turbulent channel flow and in the turbulent flow downstream of a backward-facing step. *J. Turbulence* **5**, 020.

Makel, D. & Kennedy, I. 1990 Experimental and numerical investigation of soot deposition in laminar stagnation point boundary layers. *Proc. Combust. Inst. 23:1551-1557* **23**, 1551–1557.

Messerer, A., Niessner, R. & Pöschl, U. 2003 Thermophoretic deposition of soot aerosol particles under experimental conditions relevant for modern diesel engine exhaust gas systems. *J. Aerosol Sci.* **34**, 1009–1021.

Moss, J., Stewart, C. & K.J., Y. 1995 Modeling soot formation and burnout in a high temperature laminar diffusion flame burning under oxygen-enriched conditions. *Combust. Flame* **101**, 491–500.

Nagendra, K., Tafti, D. & Viswanathan, A. 2011 Modeling of soot deposition in wavy-fin exhaust gas recirculator coolers. *Intl. J. Heat Mass Transfer* **54**, 1671–1681.

Nicoud, F. & Ducros, F. 1999 Subgrid-scale stress modelling based on the square of the velocity gradient. *Flow, Turbulence and Combustion* **62** (3), 183–200.

Pierce, C. 2001 Progress variable approach for large eddy simulation of turbulent combustion. PhD thesis, Stanford University, CA, USA.

Selle, L., Lartigue, G., Poinsot, T., Koch, R., Schildmacher, K.-U., Krebs, W., Prade, B., Kaufmann, P. & Veynante, D. 2004 Compressible large eddy simulation of turbulent combustion in complex geometry on unstructured meshes. *Combustion and Flame* **137** (4), 489–505.

Thakurta, D., Chen, M., McLaughlin, J. & Kontomaris, K. 1998 Thermophoretic deposition of small particles in a direct numerical simulation of turbulent channel flow. *Intl. J. Heat Mass Transfer* **41**, 4167–4182.

Tsai, C.-J. & Lu, H.-C. 1955 Design and evaluation of a plate-to-plate thermophoretic precipitator. *Aerosol Sci. Technol.* **22**, 172–180.

Wolf, P., R.Balakrishnan, G.Staffelbach, Gicquel, L. M. & Poinsot, T. 2012 Using les to study reacting flows and instabilities in annular combustion chambers. *Flow, Turbulence and Combustion* **88** (1-2), 191–206.